JOURNAL OF SPACECRAFT AND ROCKETS
Vol. 46, No. 3, May–June 2009

Comparison of Materials for an Integrated Thermal Protection System for Spacecraft Reentry

Christian Gogu,* Satish K. Bapanapalli,† Raphael T. Haftka,‡ and Bhavani V. Sankar§
University of Florida, Gainesville, Florida 32611-6250

DOI: 10.2514/1.35669

An integrated thermal protection system for spacecraft reentry based on a corrugated core sandwich panel concept fulfilling both thermal and structural functions is optimized for minimal mass. We seek the optimal dimensions and the best materials, but directly optimizing both continuous geometric parameters and discrete material choices is difficult. Accordingly the optimization problem is solved in two steps. In the first step, good candidate materials are selected based mainly on their thermal performance, obtained from a spline interpolation of the maximum bottom face sheet temperature. Mild simplifying assumptions allowed a reduction of the number of variables in the interpolation to two nondimensional variables. In combination with a material database, this procedure allowed a graphical comparison and selection of candidate materials. In the second step, the geometry of the integrated thermal protection system panel is optimized for different combinations of the materials identified in step one. The optimization considers both thermal and structural constraints. The lightest panel employs aluminosilicate/Nextel 720 composites for the top face sheet and web corrugation and beryllium for the bottom face sheet. For the same thermal reentry environment, this design was found to be only about 40% heavier than a reference conventional thermal protection system that does not provide any structural load carrying capabilities.

Nomenclature

A	=	cross-sectional area, m^2
Bi	=	nondimensional convection coefficient (or Biot number)
C	=	specific heat, $J/(kg \cdot K)$
d	=	thickness, mm
E	=	Young's modulus, GPa
h	=	convection coefficient, $W/(m^2 \cdot K)$
K_{IC}	=	fracture toughness, $MPa \cdot m^{0.5}$
k	=	thermal conductivity, $W/(m^2 \cdot K)$
L	=	height of the sandwich panel, mm
M	=	mass per unit area of integrated thermal protection system panel, kg/m^2
p	=	half-unit cell length, mm
q, q_i	=	heat flux, total incident heat flux, respectively, W/cm^2
T, T_i	=	temperature, initial temperature, respectively, K
t	=	time relative to the transient thermal problem, s
t_{end}	=	duration of the reentry simulation, s
$T_{\text{Max BFS}}$	=	maximum bottom face sheet temperature, K
V	=	volume, m^3
x	=	position through the thickness of the panel, m
β	=	nondimensional thermal diffusivity (or Fourier number)
Γ	=	nondimensional temperature
γ	=	nondimensional heat capacity parameter
ε	=	emissivity
θ	=	angle of corrugations, deg
κ	=	nondimensional radiation coefficient
ξ	=	nondimensional position through the panel thickness
$\boldsymbol{\rho}$	=	density, kg/m^3
σ	=	Stefan–Boltzmann constant, $W/(m^2 \cdot K^4)$
τ	=	nondimensional time
φ	=	nondimensional heat flux

Subscripts

B	=	bottom face sheet
C	=	homogenized core
S	=	Saffil® alumina foam
T	=	top face sheet
W	=	web

Presented as Paper 1860 at the 48th AIAA/ASME/ASCE/AHS/ASC Structures, Structural Dynamics, and Materials Conference, Honolulu, HI, 23–26 April 2007; received 15 November 2007; accepted for publication 6 March 2009.

*Research Assistant, Department of Mechanical and Aerospace Engineering, Post Office Box 116250; also Ph.D. Student, Ecole des Mines de Saint Etienne, France; christian.gogu@gmail.com. Student Member AIAA.

†Department of Mechanical and Aerospace Engineering, Post Office Box 116250; currently Scientist, Pacific Northwest National Lab, Post Office Box 999, Richland, Washington 99354.

‡Distinguished Professor, Department of Mechanical and Aerospace Engineering, Post Office Box 116250. Fellow AIAA.

§Ebaugh Professor, Department of Mechanical and Aerospace Engineering, Post Office Box 116250. Associate Fellow AIAA.

I. Introduction

THERMAL protection systems (TPS) are designed to protect the structure of transatmospheric space vehicles from the extreme temperatures arising during atmospheric reentry. Several TPS technologies have been developed in the past, such as ablative TPS, used mainly on the Apollo capsules [1] and interplanetary entry probes [2], or reusable TPS, based on the reinforced carbon–carbon ceramic tiles and blankets used on the space shuttle orbiter [3]. With the research for a reusable launch vehicle (RLV) [4,5], new metallic TPS concepts were developed [6,7]. Such systems, like the adaptable, robust, metallic, operable, reusable (ARMOR) TPS [6] were designed to provide a robust and reusable thermal protection system for RLV-type vehicles. This concept remains of interest for RLVs as shown in recent topology optimization studies based on the ARMOR TPS design [8].

In all the TPS concepts, a primary design factor is system weight. One potential way to achieve further weight savings can be through the concept of an integrated thermal protection system (ITPS). An ITPS would integrate the structural function of the space vehicle, providing thermal protection as well as structural load bearing capabilities compared with a conventional parasitic TPS that has

very low load bearing capabilities and is not integral to the existing structure of the vehicle. Such a multifunctional TPS structure evolves from earlier developments of metallic TPS concepts for RLV spacecraft [6,7]. Compared with a conventional TPS plus structure, such integrated designs might not be more weight efficient or even feasible for high-heat-rate reentries. Indeed the high ITPS rigidity required to fulfill the structural function poses the issue of high thermally induced stresses. For low-heat-rate environments, such as those encountered on large sections of RLV-type vehicles, the concept appeared, however, very promising in the previous studies [6,7].

Previous studies on ITPS [9,10] considered corrugated core sandwich structures (see Fig. 1) that, compared with metallic ARMOR TPS, would provide higher structural load bearing capabilities. The core of the structure is filled with Saffil® fibrous alumina foam that combines high insulation properties with low density.

Bapanapalli et al. [9] described an optimization procedure used to find the minimal mass design of this corrugated core sandwich panel ITPS structure. In this procedure, six design variables were considered, corresponding to six geometric parameters describing the sandwich structure. Each section of the ITPS [top face sheet (TFS), bottom face sheet (BFS), and corrugated web (web)] was assigned a material based on previous experience with ARMOR TPS [6] and other similar metallic TPS concepts [7]. However, there is high potential for further lowering the ITPS mass by choosing more suitable materials. The aim of the current paper is to develop a procedure for comparing potential materials for integrated thermal protection systems at the early design stages. We seek the best-suited material combination together with the corresponding optimal dimensions of the ITPS panel that would lead to a minimal mass design.

The challenge of material selection lies in the conflicting requirements of the thermal protection function and those of the structural function. Indeed, good thermal protection materials have low thermal conductivity, high heat capacity, and high service temperature. Good structural materials, on the other hand, have high strength and good fracture toughness. Typical thermal protection materials are ceramics. However, these materials are generally very poor structural materials with low strength and fracture toughness. Common structural materials are metals, which generally have high thermal conductivity and a lower service temperature, making them poor thermal protection materials. The difficulty of the material selection process lies in finding materials that provide the right combination of thermal and mechanical properties.

Optimizing simultaneously for continuous geometric parameters and discrete material choices is relatively difficult. Accordingly, we chose to proceed in two steps. In the first step, good candidate materials are selected based mainly on their thermal performance. For this purpose, in Sec. II, we employ a small number of simplifying assumptions together with a dimensional analysis and a global sensitivity analysis to construct an approximation of the maximum BFS temperature (one of the major thermal constraints) as a function of only two nondimensional parameters. In Sec. III, this approximation was used together with a material database to select good potential materials mainly from a thermal perspective. Then, in the second step, the geometry of the ITPS is optimized for minimal mass for different combinations of candidate materials found in the first step. This optimization, presented in Sec. IV, includes both structural and thermal constraints and allowed us to rank different material combinations in terms of mass. We provide concluding remarks in Sec. V.

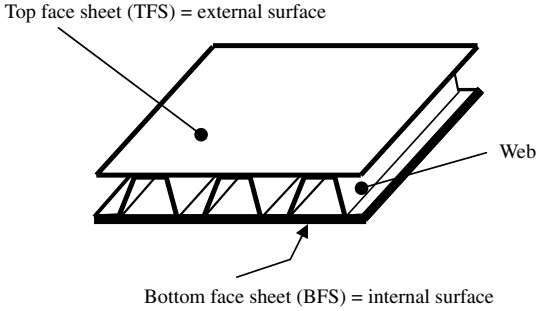

Fig. 1 Typical corrugated core sandwich panel ITPS.

II. Thermal Problem Description and Modeling

A. Thermal Problem of Atmospheric Reentry

To calculate the maximum BFS temperature, we developed a finite element (FE) model using the commercial FE software ABAQUS® [11]. The thermal problem of atmospheric reentry and the geometric parameters of the ITPS panel are shown in Fig. 2. The ITPS is subject to an incident heat flux assumed to vary as shown in Fig. 3. This heat flux is typical of the side fuselage of an RLV-type vehicle reentry [6]. Note that the considered heat flux is under the assumption of laminar flow during the reentry. The general approach presented in the present paper for material comparison would apply to different heat flux profiles.

Reradiation is also modeled on the TFS with an emissivity of 0.8, which is desirable for TPS exterior surfaces and surface treatments [12,13]. The BFS is assumed perfectly insulated (adiabatic), which, from an ITPS design perspective alone, is a worst-case assumption. Indeed, if heat could leak through the BFS, the maximum temperature would decrease, becoming less critical. The core of the sandwich panel is assumed to be filled with Saffil® fibrous alumina foam insulation, whereas we will explore different materials for the three main sections (TFS, BFS, and web).

We also assumed that, after landing, the vehicle is cooled by natural convection. The profile of the assumed convection coefficient is shown in Fig. 3. The FE thermal problem is modeled as a one-dimensional heat transfer analysis as represented in Fig. 4. The core of the sandwich panel is homogenized using the rule of mixtures formulas:

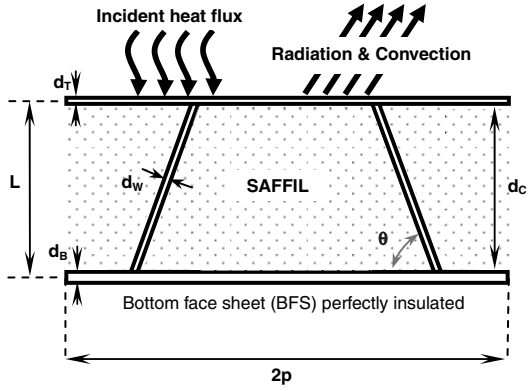

Fig. 2 Representation of the thermal problem depicting the geometric parameters of an ITPS panel unit cell.

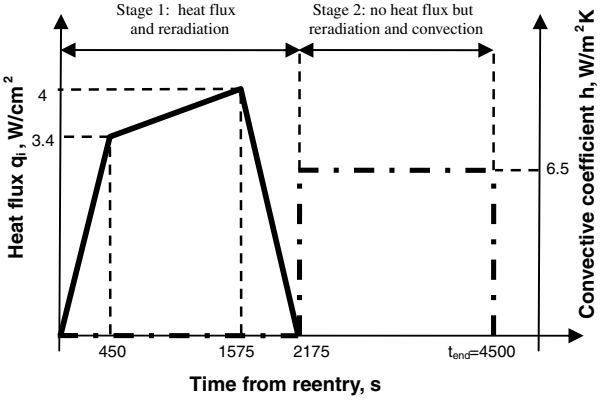

Fig. 3 Incident heat flux (solid line) and convection (dashed dotted line) profile with reentry time on the TFS surface.

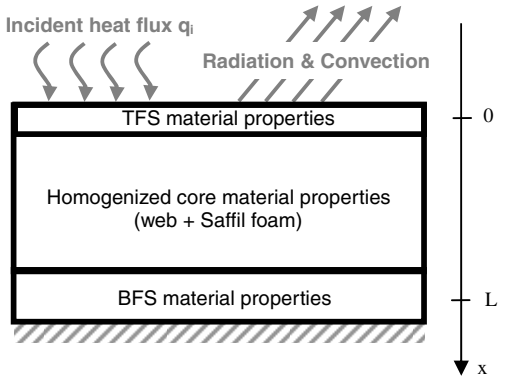

Fig. 4 One-dimensional homogenized heat transfer model.

$$\rho_C = \frac{\rho_W V_W + \rho_S V_S}{V_C} = \frac{\rho_W d_W + \rho_S (p \sin\theta - d_W)}{p \sin\theta} \tag{1}$$

$$C_C = \frac{C_W \rho_W V_W + C_S \rho_S V_S}{\rho_C V_C} = \frac{\rho_W C_W d_W + \rho_S C_S (p \sin\theta - d_W)}{\rho_W d_W + \rho_S (p \sin\theta - d_W)} \tag{2}$$

$$k_C = \frac{k_W A_W + k_S A_S}{A_C} = \frac{k_W d_W + k_S (p \sin\theta - d_W)}{p \sin\theta} \tag{3}$$

It has been shown in [9] that, for the corrugated core ITPS panel we consider, such a one-dimensional FE model can accurately predict the maximum BFS temperature. Although at the TFS large temperature differences along the surface existed due to the shorts through the web (variations of up to 90 K), this difference was significantly reduced by the time the heat flux reached the BFS. The maximum difference in maximum BFS temperature prediction between the 1- and 2-D models was found to be less than 10 K. Considering the preliminary design phase of the ITPS and because we are interested here in only the maximum BFS temperature, we found this difference acceptable.

Radiation, convection, and the incident heat flux (as shown in Fig. 2 and 3) were modeled in the ABAQUS® 1-D model using four steps: three for stage one ($t = 0$–2175 s, see Fig. 3) and one for stage two ($t = 2175$–4500 s). Fifty-four three-node heat transfer link elements were used for the transient analyses. The number of elements was found appropriate after a convergence study.

B. Approximate Temperature Determination and Validation

Using the previously described finite element model to compare all possible material combinations one by one would be too computationally expensive. Accordingly, we want to construct an approximation of the maximum BFS temperature, which would facilitate the material selection process. To make this approximation as time efficient as possible, we want to express the approximate maximum BFS temperature function of the smallest possible number of parameters. Ideally, we want to be able to express the approximation function of two parameters or less, which would also allow graphical representation of the results and, thus, make the material selection more user friendly.

The thermal model presented in the previous section involves 13 material parameters (specific heat C, conductivities k, and densities ρ of the TFS, BFS, web, and Saffil®, as well as the emissivity ε of the TFS) of which most are temperature dependent. Some of these parameters were fixed during this study, including ε as well as all the foam parameters. The foam material was fixed to Saffil®, which has been determined in previous studies [6,7] to be the best-suited foam in similar metallic thermal protection systems. The emissivity of the TFS was also fixed because it depends more on surface treatments than on the nature of the TFS material (a typical value for this kind of application of 0.8 was used [7,12]). Fixing these parameters leaves nine parameters of interest to come from the material selection (specific heat C, conductivities k, and densities ρ of the TFS, BFS, and web). Our immediate goal now is to condense these nine parameters into the smallest number possible.

On a mildly simplified analytical model of the thermal problem, we used nondimensionalization, which together with a global sensitivity analysis allowed us to determine that the maximum BFS temperature could be approximately expressed as a function of only two nondimensional parameters, β and γ (see Appendix A for details). Equations (4) and (5) give their expressions.

$$\beta = \frac{\frac{k_C t_{\text{end}}}{d_C}}{d_C \rho_C C_C} = \frac{k_C t_{\text{end}}}{d_C^2 \rho_C C_C} \tag{4}$$

$$\gamma = \frac{d_B \rho_B C_B}{d_C \rho_C C_C} \tag{5}$$

Parameter β (the Fourier number) is a nondimensional thermal diffusivity, that is, the ratio between the rate of heat conduction and the rate of heat storage (thermal energy storage) of the homogenized core; parameter γ is the ratio between the heat capacity of the BFS and heat capacity of the homogenized core.

We can substitute the material parameters of the homogenized core from Eqs. (1–3) back into the expressions of β and γ from Eqs. (4) and (5), which yields expressions (6) and (7). This shows directly the dependence of β and γ on the nine material properties of the different ITPS sections (specific heat C, conductivities k, and densities ρ of the TFS, BFS, and web) as well as the dependence on the six geometry parameters (shown in Fig. 2), a total of 15 parameters. For a more detailed view of nondimensionalization and the simplifying assumptions that allowed us to reduce the number of variables, refer to Appendix A.

$$\beta = \frac{k_C t_{\text{end}}}{d_C^2 \rho_C C_C} = \frac{[k_W d_W + k_S (p \sin\theta - d_W)] \cdot t_{\text{end}}}{(L - 0.5 d_T - 0.5 d_B)^2 \cdot [\rho_W C_W d_W + \rho_S C_S (p \sin\theta - d_W)]} \tag{6}$$

$$\gamma = \frac{d_B \rho_B C_B}{d_C \rho_C C_C} = \frac{d_B \rho_B C_B p \sin\theta}{(L - 0.5 d_T - 0.5 d_B) \cdot [\rho_W C_W d_W + \rho_S C_S (p \sin\theta - d_W)]} \tag{7}$$

We would now like to check if the accurate maximum BFS temperature coming from the finite element analyses can also be expressed with good accuracy as a function of only β and γ (which were determined on an approximate analytical model).

By varying t_{end} in β and d_B in γ, we constructed an 11×11 grid in β and γ within the bounds $\beta \in [0.1; 0.5]$ and $\gamma \in [0.6; 2.4]$. We ran the corresponding 121 finite element simulations and used a cubic spline interpolation to calculate the temperature between these points. The corresponding maximum BFS temperature function of β and γ is plotted in Fig. 5.

To determine the error resulting from using only two variables instead of the initial 15 (nine materials properties and six geometric parameters), we compared the temperature predictions from the two-dimensional spline interpolation with the FE analyses at 285 Latin hypersquare points spread in the 15-dimensional variables space. The 285 points were constructed so that the corresponding β and γ of these points fall inside the range used for the grid: $\beta \in [0.1; 0.5]$ and $\gamma \in [0.6; 2.4]$. The mean of the absolute difference between the finite element analyses and the two-dimensional spline temperature predictions was 2.52 K with a standard deviation of 2.23 K, while the maximum difference observed among the 285 points was 11.2 K (the range of the temperatures is about 250 K).

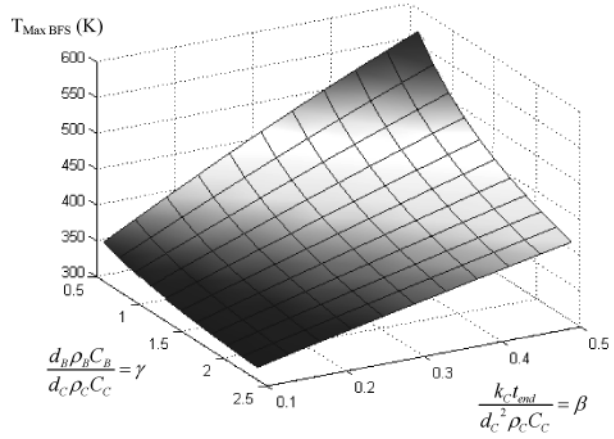

Fig. 5 Maximum BFS temperature plot function of the two nondimensional variables.

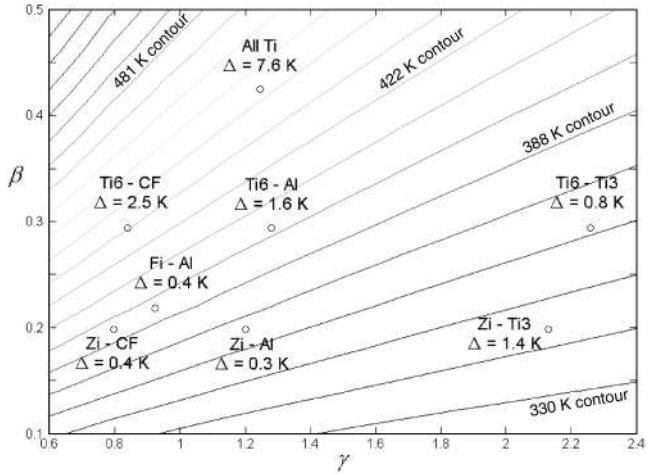

Fig. 6 Absolute error Δ of the two-dimensional interpolation prediction compared with FE analyses for different material combinations (see Table 1 for legend).

The two-dimensional temperature approximation will be used in the succeeding sections for material selection, and so it was also tested with eight representative material combinations for the ITPS. This test evaluates the error of condensing the initial 15 parameters into only two, but this time with actual materials, whereas the previous test used random material property values. On the other hand, the previous test was more general because it varied both the material properties and geometric parameters simultaneously, whereas the geometry is fixed in this second test.

The results of the second test are illustrated in Fig. 6, with the test points plotted in the (β, γ) plane along with the corresponding temperature errors compared with the FE analyses. The maximum BFS temperature (from the interpolation) is superimposed as a contour plot. The format for the designations of the material combinations tested is web material/BFS material (see Table 1 for full designations). The TFS material is aluminosilicate/Nextel 720 composites except in the reference all-titanium design, in which it is Ti-6Al-4V. Saffil® was used each time as filler insulation, as previously noted. The geometry of the ITPS is fixed and given in Table 2. The mean of the error was 2.1 K, and the maximum error among the test points was 7.6 K (the range of the temperature test points is about 100 K). From these tests we concluded that the error induced by using only the two nondimensional parameters instead of the initial 15 is acceptable for the first step of the material selection procedure.

III. Initial Material Comparison and Screening

Having the two-dimensional approximation of the maximum BFS temperature, which accounts for all the material parameters we are interested in, we now want to compare different material combinations for their ability to lead to a low maximum BFS temperature. The two-dimensional nature of the approximation allows us to represent the temperature for different materials graphically.

In this entire section, the geometric parameters were kept fixed at the values given in Table 2. These values were found in [9] to be optimal for an Inconel 718 (TFS), Ti6Al4V (web), Al (BFS) ITPS panel. Reoptimization for the materials that we find in this section will be done during the second step presented in Sec. IV.

To check through a wide range of materials, we used CES Selector 2005 [14]. This is a material selection software based on a database of over 3000 materials ranging from polymers to ceramics and through the full range of metal alloys. It allows searching for materials while imposing bounds on the material parameters. Combined with the spline interpolation, it allowed the graphical comparison and selection of potential materials for each section of the ITPS panel at low computational cost. Note that, although the software is not free, the properties of the materials that were selected and later used in this study are provided in Appendix B.

A. Web Material Comparison

The web of the ITPS has to resist very high temperatures because its upper part is at the same temperature as the TFS. Accordingly, we assumed a limit of 1173 K (900°C) for the maximum service temperature. This is about 200 K higher than the maximum temperature of the TFS for the heat flux considered (see Fig. 3), but was chosen to allow potential changes of the heat flux profile. At the same time, the web is a structural part, which imposes constraints on Young's modulus and the fracture toughness. Finally, the web must be as light as possible, imposing an upper limit on the density. Accordingly, the following requirements were imposed during the search for materials suitable for the web:

$$\begin{aligned}&\text{Min. acceptable max. service temp. } T_{\max\ \text{service}} > 1173\ \text{K}\\&\text{Young's modulus } E > 50\ \text{GPa}\\&\text{Fracture toughness } K_{IC} > 10\ \text{MPa}\cdot\text{m}^{0.5}\\&\text{Density } \rho < 6000\ \text{kg/m}^3\end{aligned} \tag{8}$$

It should be noted that the only purpose of the requirements on E, K_{IC}, and ρ was to avoid the selection of materials that were good from a thermal point of view but extremely poor from a mechanical point of view (foams, for example). The true structural constraints were imposed during the coupled thermomechanical optimization presented in Sec. IV.

A total of 127 materials satisfying these requirements were found in the database. A large majority of these materials could be classified as austenitic steels, nickel–chromium alloys, or cobalt base superalloys. The 127 materials are plotted in Fig. 7, some grouped under the classifications above (these regrouped materials are denoted with an asterisk on the plot). For the plot, the ITPS dimensions are fixed and given in Table 2 and the BFS material is fixed to aluminum alloy 2024. The figure shows the different materials in the (β, γ) plane with the contours of the maximum BFS temperatures (obtained from the spline inter-

Table 1 Material combinations considered for testing the spline interpolation, where CF denotes carbon fiber

Designation	Web	BFS
All Ti	Ti–6Al–4V alloy	Ti–6Al–4V alloy
Ti6–CF	Ti–6Al–5Zr–0.5Mo alloy	Graphite/epoxy composites
Ti6–Al	Ti–6Al–5Zr–0.5Mo alloy	Aluminum 2024 alloy
Ti6–Ti3	Ti–6Al–5Zr–0.5Mo alloy	Ti–3Al–5Mo alloy
Fi–Al	Fictitious material	Aluminum 2024 alloy
Zi–CF	Zirconia	Graphite/epoxy composites
Zi–Al	Zirconia	Aluminum 2024 alloy
Zi–Ti3	Zirconia	Ti–3Al–5Mo alloy

Table 2 Dimensions of the ITPS used during the thermal material selection process. Dimensions were optimal for an Inconel 718 (TFS), Ti–6Al–4V (web), Al (BFS) ITPS [9]

Parameter	d_T, mm	d_B, mm	d_W, mm	θ, deg	L, mm	p, mm
Value	2.1	5.3	3.1	87	120	117

polation) superimposed to allow comparison of their thermal performance (i.e., low maximum BFS temperature).

We seek web materials leading to low BFS temperatures, which implies high insulation capabilities. We can see that materials such as aluminosilicate/Nextel 720 composites or zirconia ceramics provide a significant reduction in the maximum BFS temperature compared with metals such as titanium alloys, which were considered in previous designs [9]. A possible drawback of zirconia is its relatively low fracture toughness. Still, aluminosilicate/Nextel 720 composites and zirconia were selected as good candidates for the web to be further compared through the thermomechanical optimization that will be presented in Sec. IV. Their material properties are listed in Appendix B.

B. Bottom Face Sheet Material Comparison

A similar approach was taken for the BFS materials comparison. The BFS must act as a heat sink, and its temperature cannot exceed a value required for the mission operation (typically a limit of 450 K for aluminum structures). The same limits on the mechanical properties were imposed as previously. In total, we have the following requirements:

$$\begin{aligned}&\text{Min. acceptable max. service temp. } T_{\max\ \text{service}} > 450\ \text{K}\\ &\text{Young's modulus } E > 50\ \text{GPa}\\ &\text{Fracture toughness } K_{IC} > 10\ \text{MPa}\cdot\text{m}^{0.5}\\ &\text{Density } \rho < 6000\ \text{kg/m}^3\end{aligned} \tag{9}$$

A total of 235 materials satisfied these requirements, and these materials were plotted in the $(\rho_B C_B, \rho_B)$ plane for a web material fixed to a Ti–6Al–5Zr–0.5Mo alloy. The BFS material affects only γ, not β, and so a one-dimensional plot function of $\rho_B C_B$, which is proportional to γ, would have been sufficient. We chose to add ρ and have a plot in the $(\rho C, \rho)$ plane to show how much of $\rho_B C_B$ is due to the density and how much to the specific heat, because weight is critical in the ITPS design. Thus, we have two objectives: lowest possible maximum BFS temperature and lowest possible weight. This will allow us to define a Pareto front for the materials. A material is Pareto optimal and thus belongs to the Pareto front if it is not possible to find another material that improves one objective without deteriorating the other one. The results are shown in Fig. 8 (an asterisk denotes generic material names regrouping several actual materials). For the plot, the ITPS dimensions are fixed to the values in Table 2 and the web material is fixed to a Ti–6Al–5Zr–0.5Mo alloy.

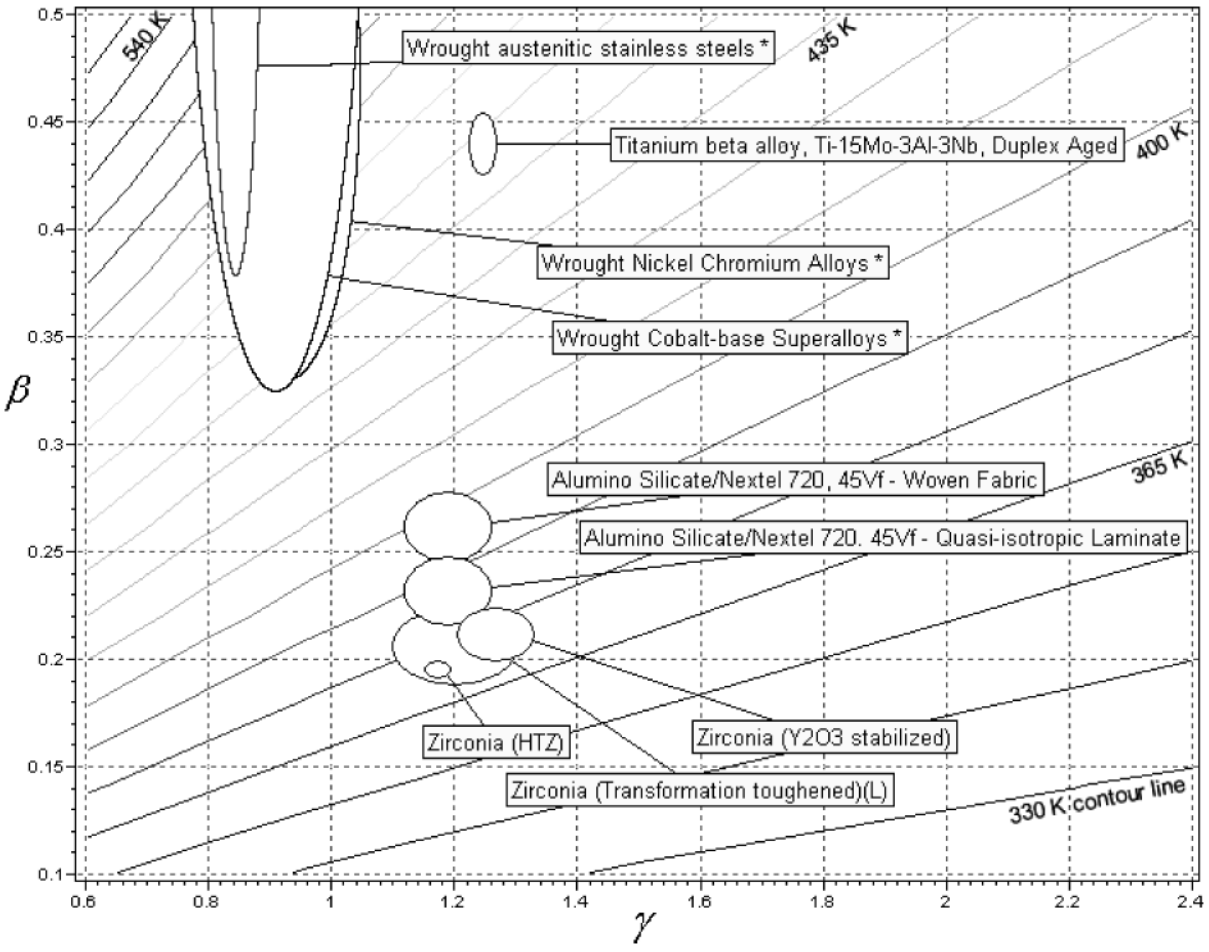

Fig. 7 Thermal comparison of materials suitable for the web, that is, satisfying the requirements in Eq. (8); the contours of the maximum BFS temperature are shown in the background. (The asterisks denote materials regrouped under a generic material name.)

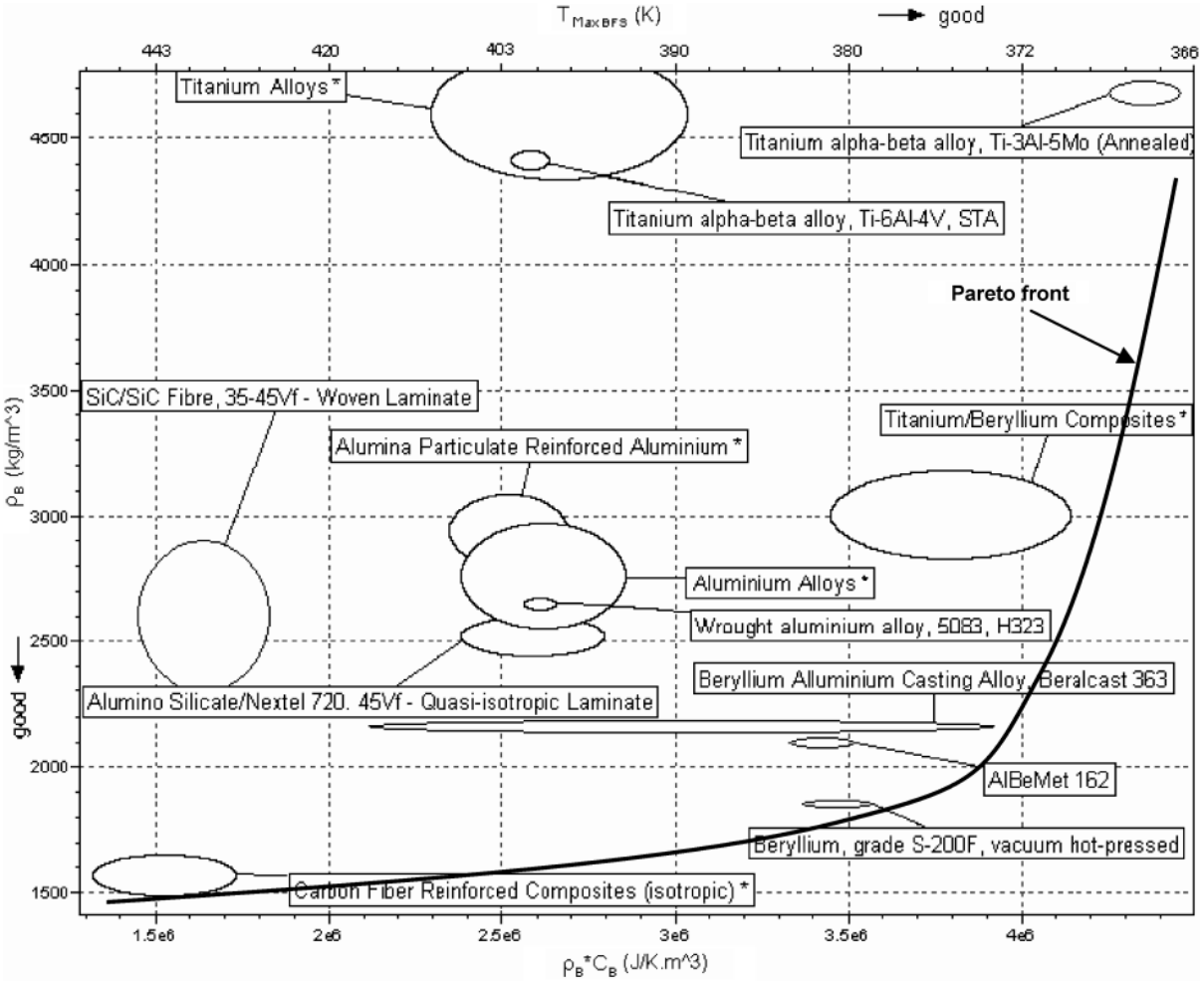

Fig. 8 Thermal performance comparison of materials suitable for the BFS, that is, satisfying the requirements in Eq. (9). (The asterisks denote materials regrouped under a generic material name.)

We seek lightweight materials (bottom of the y axis) leading to a low maximum BFS temperature (right of the top x axis). The top axis shows for each $\rho_B C_B$ value the corresponding maximum BFS temperature (obtained from the spline interpolation). Note that this scale is nonlinear.

For the BFS selection, the choice of materials is larger than for the web. We chose to concentrate on low-density materials due to weight considerations. The best materials for the BFS from a thermal as well as mass point of view are beryllium-based materials. Beryllium has very high specific heat and low density, which is ideal for BFS use. The major drawbacks of beryllium are its toxicity during manufacturing as well as its relatively low fracture toughness. Alternative BFS materials are aluminum alloys, which was the material used in [9]. Carbon-fiber-reinforced composites are the lightest materials (almost twice as light as aluminum alloys), but they have a 40 K penalty with respect to their corresponding maximum BFS temperature. Beryllium S-200F, aluminum alloy 2024, and graphite/epoxy composites (included in the figure under the designation "carbon-fiber-reinforced composites") were selected as good candidates for the BFS to be further compared through the thermomechanical optimization in Sec. IV. Their material properties are listed in Appendix B.

C. Top Face Sheet Material Comparison

The TFS material has a negligible effect on the maximum BFS temperature (see Appendix A for detailed explanations). This means that the selection of the TFS material will not be based on the maximum BFS temperature. Instead, the TFS is subjected to the following requirements. It reaches high temperatures, and so the maximum service temperature of the material must be higher than the temperatures experienced (typically 900–1200 K depending on the maximum heat flux); a value of 1173 K (900°C) was chosen here as the requirement for the TFS material. The TFS is also very likely to buckle due to the thermally induced stresses involved at these high temperatures, requiring high buckling resistance, which translates to an elevated Young's modulus. The TFS, being the exterior part of the spacecraft, would also have to withstand potential impacts (either during ground handling or due to micrometeoroids), which was translated into a requirement for a fracture toughness higher than that imposed for BFS and web.

Because Young's modulus and the maximum service temperature drive the material selection for the TFS, we plot the materials in the maximum service temperature/Young's modulus plane while imposing the following requirements on the materials represented:

$$\begin{aligned}&\text{Min. acceptable max. service temp. } T_{\max\ \text{service}} > 1173\ \text{K}\\&\text{Young's modulus } E > 50\ \text{GPa}\\&\text{Fracture toughness } K_{IC} > 15\ \text{MPa}\cdot\text{m}^{0.5}\\&\text{Density } \rho < 6000\ \text{kg/m}^3\end{aligned} \tag{10}$$

Only five materials in the CES Selector database satisfied these requirements. These materials are plotted in Fig. 9. Carbon–carbon composites have been also added to the figure even though, according to the database, they do not satisfy the fracture toughness requirement. However, this material is currently used as part of the thermal protection system of the space shuttle orbiter, and advanced carbon–carbon composites might be a potential candidate for the TFS in our application.

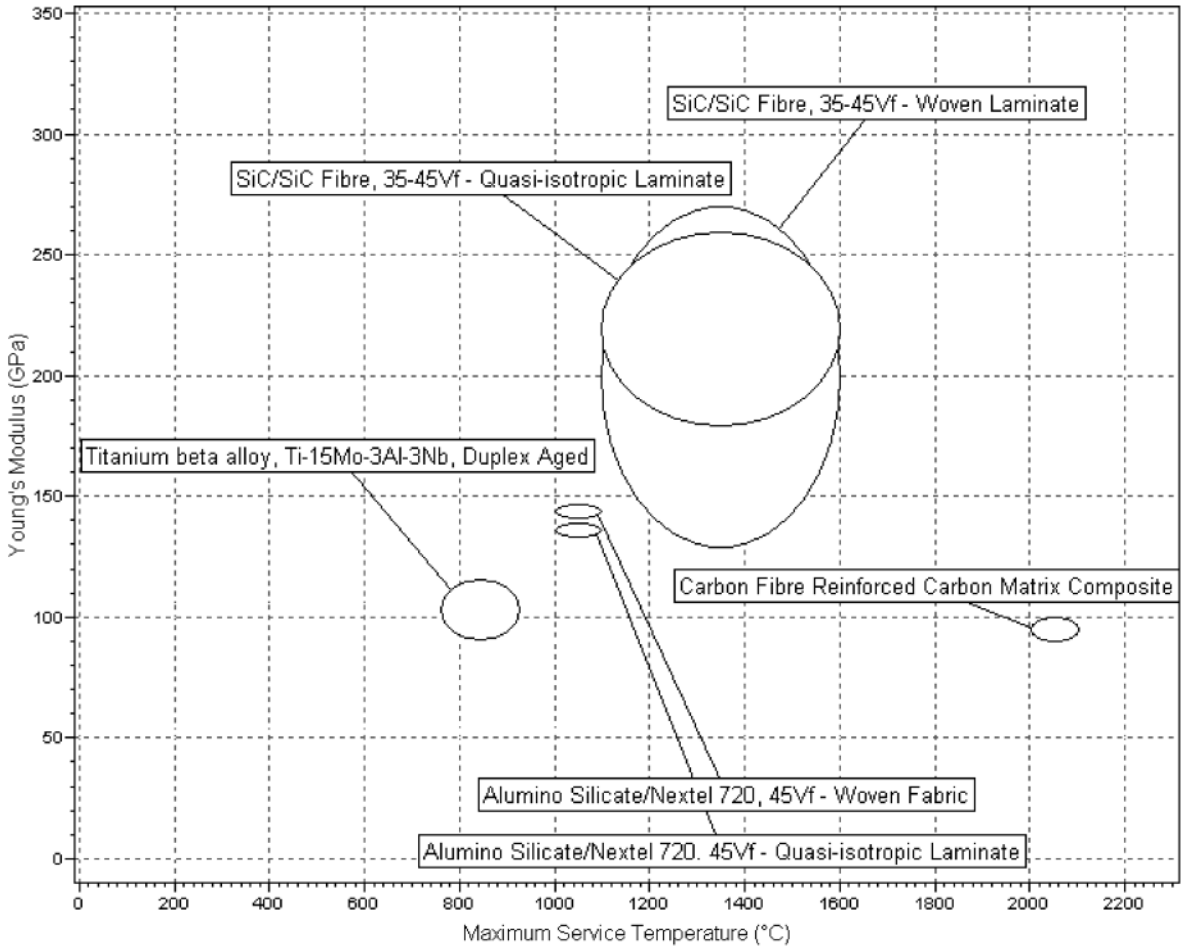

Fig. 9 Potential materials for the TFS, that is, satisfying the requirements in Eq. (10).

Carbon–carbon composites have a very high maximum service temperature while still having a reasonably high Young's modulus. Their major drawback is their fracture toughness and, considering that this was a contributing factor to the Space Shuttle Columbia disaster [15], we sought alternative materials for the TFS. Silicon carbide (SiC) composites are another candidate for the TFS but they have, though to a lesser extent, the same fracture toughness issue as carbon–carbon composites.

Aluminosilicate/Nextel 720 composites are the next possible choice with a good maximum service temperature and Young's modulus. They also have much higher fracture toughness (more than 40 MPa $\cdot$ $m^{0.5}$) than the previous two materials. Accordingly, aluminosilicate/Nextel 720 composites were selected as the TFS material for the coupled thermomechanical optimization that will be presented in the next section. Their material properties are listed in Appendix B.

IV. Coupled Thermomechanical Optimization of the Geometry of the Integrated Thermal Protection System

In the previous section we obtained a small number of good candidate materials for each section of the ITPS (BFS, web, and TFS). The next step in the material selection process is to include structural constraints and optimize the geometry for minimal mass for different combinations of the candidate materials found.

Indeed, in the previous sections the geometry was fixed, and so it was not guaranteed that the ITPS dimensions corresponded to a minimal mass design. Also, even though some mechanical constraints were considered during the database search of the previous sections, the material selection was done primarily from a thermal point of view. In this section, structural constraints are directly imposed through limits on the buckling eigenvalues, local buckling being found to be the most likely failure mode of the ITPS sandwich panel structure. After optimization, the different material combinations are ranked with respect to their mass.

A. Optimization Problem

The geometry optimization was done using a previously developed optimization procedure, which will be briefly described here. For more details, refer to [9]. The ITPS panel geometry is parameterized in terms of L, p, θ, d_T, d_B, and d_W (see Fig. 2). These parameters are selected as the design variables.

The aim of the optimization is to minimize the mass per unit area of the ITPS panel under the following constraints: a maximum BFS temperature of $<$450 K and a smallest buckling eigenvalue of $>$1.25 (which includes a 25% safety factor).

We can note that constraints for stresses and deflections were not considered during the optimization. This decision was based on initial analyses on an Inconel 718(TFS), Ti–6Al–4V(web), Al 2024 (BFS) ITPS design, which showed that these constraints were not active by a large margin, whereas the maximum BFS temperature and buckling eigenvalues were the active constraints.

To implement these active constraints in the optimization, response surface approximations (RSAs) were used for both the temperature and the buckling constraints to reduce computational cost.

The maximum BFS temperature RSA was based on the FE model, described in Sec. II.A, with temperature-dependent material properties. We used 180 Latin hypersquare sample points to construct a cubic polynomial RSA function of the six geometry variables. This RSA in the six geometry variables (denoted RSA6) was used instead of the two nondimensional variables interpolation (denoted here SPL2) described in Sec. II. This choice was mainly because the procedure for obtaining RSA6 and coupling it to the optimization was already developed [9] and the computational time

for constructing the thermal RSA is small compared with the time needed for the buckling RSAs, and so no significant time savings could have been achieved by switching the thermal RSA from RSA6 to SPL2. Furthermore, RSA6 was found to be more accurate than SPL2 (lower rms error) and the FE analyses conducted for RSA6 were needed in any case to obtain the distribution of the temperature through the thickness of the ITPS as input for the structural analysis.

B. Finite Element Model for the Buckling Constraint

The smallest buckling eigenvalue constraint concerns local buckling of the different sections of the ITPS (TFS, web, or BFS), with local buckling being the most likely structural failure mode (see Fig. 10 for an example of a local buckling mode). Accordingly, response surface approximations of the smallest buckling eigenvalue were determined for each section of the ITPS (TFS, web, and BFS) at four different critical times: 1) time 1: time of maximum thermal gradient, 2) time 2: time when the TFS reaches its maximum temperature, 3) time 3: time when the BFS reaches its maximum temperature, and 4) time 4: time when the midpoint of the web reaches its maximum temperature.

The response surface approximations were constructed using a finite element model at the same 180 Latin hypersquare points as the temperature response surface approximation. A cubic polynomial response surface was used.

The ABAQUS® finite element model for the buckling analysis is a 3-D model of one-quarter of the ITPS panel (using symmetry boundary conditions). The model uses a total of 1820 eight-node shell elements (S8R). The boundary conditions considered are 1) fixed vertical displacements and rotations on the edges of the BFS, and 2) only fixed rotations on the TFS edges. The fixed rotations boundary conditions at the TFS can be explained by the way the panels are attached to each other through slots, which allow in-plane displacements but not rotations. Again, for more details refer to [9].

C. Optimal Design Results for Different Material Combinations

Different material combinations based on the good potential candidate materials found in Sec. III could now be submitted to the geometry optimization. The material sets considered are given in Table 3. The first material combination (Inc–Ti–Al) is the reference set; this is the combination that was used previously for the ITPS [9].

The optimization for each of these material sets was done in a sequential way. The first optimization started with a set of large initial bounds on the six design variables. The corresponding optimal design was found and checked with a finite element analysis. If the predicted optimal design was found to satisfy the constraints with an acceptable accuracy, the design was kept; otherwise, an optimization was repeated with reduced bounds around the previous optimum design until a sufficiently accurate optimal design prediction was obtained. The bounds used in the final optimization for each material set are given in Table 4. The corresponding optimal designs for each material set are presented in Table 5, and the FE verification of the optimal design points is given in Table 6. The errors in the RSA constraints at the optimal points were, at worst, 6.4% for the critical buckling eigenvalues, whereas the temperature RSA always had excellent accuracy (less than a 0.2% error). These errors were considered acceptable for the purpose of this study.

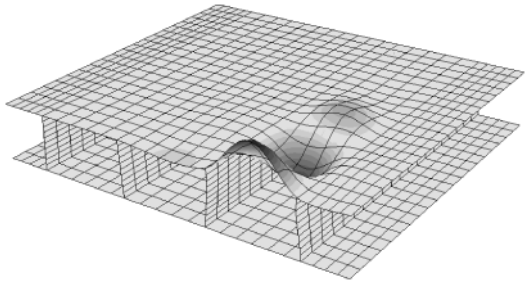

Fig. 10 Typical local buckling mode (here TFS buckling). Only one-quarter of the panel is represented by symmetry.

D. Discussion of Optimal Designs

Figure 11 summarizes in a graphical form the information in Table 5, providing the weight of the different material combinations and their distribution among the three sections of the panel.

The reference material set Inc–Ti–Al represents the design used in [9] before this systematic material comparison study was carried out. The material choice of Inconel 718 alloy for TFS, Ti–6Al–4V alloy for web, and aluminum 2024 alloy for BFS was made based on previous experience with metallic TPS, such as ARMOR [6,7]. However, there are significant structural differences between the ARMOR TPS and the corrugated core sandwich panel ITPS considered here, which make this material choice less than optimal in our case.

Material set Nex–Ti–Al shows the advantage of using aluminosilicate/Nextel 720 composites for the TFS compared with Inconel 718 in that we can save about 50% mass. This significant improvement is because Nextel 720 composites have about 3 times lower density compared with Inconel 718; it also reduces the thermal mismatch between the TFS and the web, which alleviates buckling and makes it possible to have much lower thicknesses for these two sections. The lower web thickness reduces the heat flow to the BFS and allows reduction in its thickness as well.

An additional 22% improvement in mass can be obtained by switching the web material to zirconia, which is a better thermal insulator than titanium, reducing the heat flow through the core of the ITPS. Nextel 720 composites for the web allow further weight savings, mainly due to their much lower density compared with zirconia.

Alternative BFS materials also provide additional mass savings. We can note that graphite/epoxy composites, having relatively poor heat capacity, lead to designs that concentrate a low relative mass in the BFS. Beryllium, on the other hand, has much better heat capacity combined with a low mass density, which leads to very light designs.

Overall, the lowest mass design is obtained with a Nextel 720 composites (TFS), Nextel 720 composites (web), beryllium (BFS) material combination, which leads to a mass per unit area of 12.0 kg/m^2 (2.47 lb/ft^2). Nextel 720 composites provide a good maximum service temperature for use in the TFS as well as low heat conduction for the web while at the same time having good thermomechanical properties and a low mass density, which is beneficial for both TFS and web. Beryllium in the BFS provides an excellent heat sink while still having very low mass density combined with appropriate thermomechanical properties.

We chose to compare the mass of this Nextel 720 composites (TFS and web), beryllium (BFS) ITPS with that of a conventional TPS providing thermal protection but no structural capabilities. Note that it is difficult to compare the ITPS, which is in a preliminary design stage, to any existing TPS designs without biasing the comparison. Therefore, we chose to make the comparison with a reference TPS-only design that would be at the same design stage. The TPS-only system was defined and sized as follows. Starting from the baseline corrugated core design, we reduced the thickness of the web to a minimum (0.05 mm thick). This makes the web lose any structural function and become only a thin foil keeping the Saffil® insulation in place. We also fixed the TFS to a 0.5-mm-thick Nextel 720 composite sheet and the BFS to a 2.54-mm-thick aluminum sheet. These are typical thicknesses and resulting masses that are used in conventional TPS designs [13]. For the same thermal environment as the ITPS (see Fig. 3), we then sized the thickness of this TPS-only panel to satisfy the 450 K temperature constraint on the BFS. We obtained a total panel thickness of 128 mm, and the corresponding mass of the TPS-only system was 8.31 kg/m^2 (1.7 lb/ft^2). This mass does not include the spacecraft structure. The lightest ITPS design we found is about 44% heavier. However, whereas the TPS-only design provides only thermal protection capabilities, the ITPS concept provides additional structural-load-bearing capabilities through the corrugated core sandwich panel concept.

Table 3 Material combinations considered for optimization

Designation	TFS	Web	BFS
Inc–Ti–Al (reference set)	Inconel 718 alloy	Ti–6Al–4V alloy	Aluminum 2024 alloy
Nex–Ti–Al	Aluminosilicate/Nextel 720 composites	Ti–6Al–4V alloy	Aluminum 2024 alloy
Nex–Zi–Al	Aluminosilicate/Nextel 720 composites	Zirconia	Aluminum 2024 alloy
Nex–Zi–CF	Aluminosilicate/Nextel 720 composites	Zirconia	Graphite/epoxy composites
Nex–Nex–CF	Aluminosilicate/Nextel 720 composites	Aluminosilicate/Nextel 720 composites	Graphite/epoxy composites
Nex–Zi–Be	Aluminosilicate/Nextel 720 composites	Zirconia	Beryllium
Nex–Nex–Be	Aluminosilicate/Nextel 720 composites	Aluminosilicate/Nextel 720 composites	Beryllium

Table 4 Bounds used during the final optimizations, where LB and UB are the lower and upper bounds, respectively

Material set	d_T. mm		d_B, mm		d_W, mm		θ, deg		L, mm		p, mm	
	LB	UB	LB	UB	LB	UB	LB	UB	LB	UB	LB	UB
Inc–Ti–Al	1.50	3.30	5.10	7.30	2.40	4.40	87	90	110	150	115	150
Nex–Ti–Al	1.00	1.70	4.00	5.00	1.30	2.20	87	90	90	130	115	150
Nex–Zi–Al	1.00	1.60	2.60	3.50	1.05	2.00	87	90	65	105	110	150
Nex–Zi–CF	0.50	0.90	2.20	3.00	1.60	2.30	87	90	95	125	120	150
Nex–Nex–CF	1.15	1.85	1.60	2.40	1.55	2.15	87	90	100	145	100	150
Nex–Zi–Be	1.00	1.60	1.80	2.60	0.90	1.50	87	90	65	100	110	150
Nex–Nex–Be	1.20	1.80	2.00	2.75	1.10	1.70	87	90	70	105	110	150

Table 5 Optimal geometry ITPS designs for the different material sets enumerated in Table 3

	d_T, mm	d_B, mm	d_W, mm	L, mm	M, kg/m^2 (lb/ft^2)	M_T, kg/m^2	M_C[a], kg/m^2	M_B, kg/m^2
Inc–Ti–Al (reference)	2.32	5.84	2.86	113	47.0 (9.63)	19.0	11.8	16.2
Nex–Ti–Al	1.59	4.94	1.33	95.0	23.3 (4.78)	3.90	5.79	13.6
Nex–Zi–Al	1.28	3.27	1.28	82.0	18.2 (3.73)	3.13	6.03	9.05
Nex–Zi–CF	0.78	2.67	2.08	110	17.8 (3.64)	1.91	11.7	4.20
Nex–Nex–CF	1.51	2.34	1.87	128	14.2 (2.90)	3.70	6.84	3.63
Nex–Zi–Be	1.27	2.25	1.20	80.9	13.0 (2.66)	3.12	5.74	4.14
Nex–Nex–Be	1.52	2.48	1.40	81.4	12.0 (2.47)	3.73	3.71	4.56

[a]Note: M_C represents the mass of the homogenized core (i.e., web + Saffil). Corrugation angle θ and the length of half-unit cell p went to the upper bound, 90 deg and 150 mm, respectively, for all material sets.

Table 6 Comparison of RSA predictions vs actual FE values at the optimal design point for the different material sets; for the buckling eigenvalues, the section in which buckling occurs is given in parentheses

		T_{MaxBFS}, K	Buckling at time 1	Buckling at time 2	Buckling at time 3	Buckling at time 4
Inc–Ti–Al	Predicted	450	1.25 (TFS) 1.25 (web)	1.25 (web)	2.73 (web)	1.42 (web)
	Actual	451	1.23 (TFS) 1.24 (web)	1.23 (web)	2.72 (web)	1.41 (web)
Nex–Ti–Al	Predicted	450	1.25 (web)	2.83 (web)	1.25 (TFS)	2.94 (web)
	Actual	450	1.21 (web)	2.61 (web)	1.17 (TFS)	2.62 (web)
Nex–Zi–Al	Predicted	450	1.25 (TFS) 1.25 (web)	3.68 (web)	1.25 (TFS)	3.32 (BFS)
	Actual	450	1.17 (TFS) 1.18 (web)	3.53 (web)	1.19 (TFS)	3.32 (BFS)
Nex–Zi–CF	Predicted	450	1.25 (TFS)	1.61 (web)	1.48 (web)	1.25 (web)
	Actual	450	1.21 (TFS)	1.61 (web)	1.48 (web)	1.26 (web)
Nex–Nex–CF	Predicted	450	1.25 (TFS)	2.74 (web)	1.25 (web)	1.45 (web)
	Actual	451	1.27 (TFS)	2.76 (web)	1.23 (web)	1.44 (web)
Nex–Zi–Be	Predicted	450	1.25 (web)	4.06 (web)	1.25 (TFS)	4.04 (web)
	Actual	449	1.23 (web)	4.03 (web)	1.22 (TFS)	4.02 (web)
Nex–Nex–Be	Predicted	450	1.25 (TFS) 1.25 (web)	2.02 (web)	1.25 (TFS)	2.00 (web)
	Actual	450	1.21 (TFS) 1.24 (web)	1.98 (web)	1.24 (TFS)	1.96 (web)

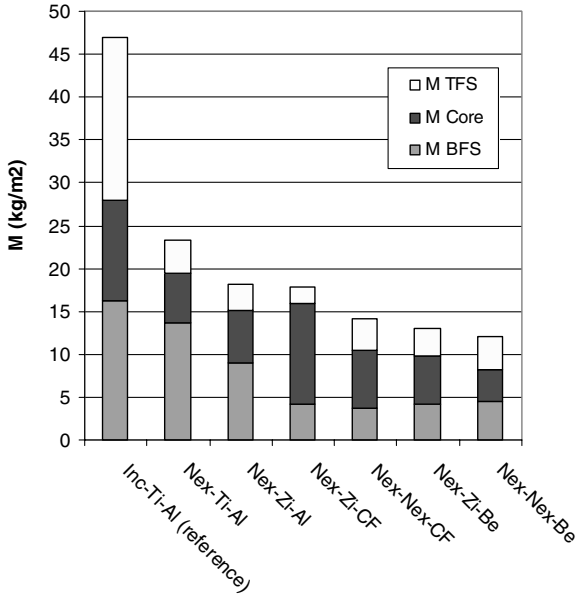

Fig. 11 Graphical representation of the mass distribution for the optimal geometry designs of different material sets.

The Nextel 720 composites (TFS and web), beryllium (BFS) ITPS was found to withstand in-plane loads of 3.0×10^5 N/m (a typical load for X-33 RLV-type vehicles) with a safety factor of 2.47 for the critical buckling failure. Note that the mass comparison figure obtained (44% mass increase) is application specific. It was obtained for the corrugated core ITPS design and thermal reentry conditions described in Sec. II.A. Although it can not be generalized, it is, however, an indicator of potential mass savings achievable with an integrated design.

Beryllium, which is used in the BFS of the lightest ITPS design we found, could pose issues during manufacturing, in particular relative to beryllium's toxicity. If we want to use a less exotic material for the BFS, we can note that the design with Nextel 720 composites (for TFS and web) and graphite/epoxy composites for BFS leads to a mass of 14.2 kg/m^2 (2.9 lb/ft^2), which is about 18% heavier than the beryllium BFS design.

We note at this point that no manufacturing constraints have been considered in this study. Manufacturing would probably be a major design problem by itself, but would probably be very specific to the materials chosen. If one of the designs determined here is found to be appealing enough, additional studies would then be necessary to investigate the best way of manufacturing and how to avoid other issues such as stress concentrations and the attachment of the sections to each other and to the vehicle.

V. Conclusions

A material selection study for an ITPS was presented that sought material combinations together with the corresponding optimal panel geometry for low-mass designs. For this purpose, a two-step approach was used.

In the first step, good potential materials were selected mainly from a thermal perspective. For this purpose, an approximation of the maximum BFS temperature of the ITPS panel was constructed using several simplifying assumptions, a dimensional analysis, and a global sensitivity analysis for reducing the number of variables relevant for the maximum BFS temperature from 15 to 2. It was found that this approximation in terms of the two nondimensional variables is relatively accurate (for our use and, over a range of 250 K, the error was less than 7.6 K compared with analyses not using any of the simplifying assumptions). The two-dimensional approximation was used in combination with a search in a materials database to find the most promising materials. Then, in the second step, a coupled thermomechanical optimization of the geometry of the ITPS, using both thermal and structural constraints, allowed us to rank the different material combinations with respect to mass.

We found that the materials selection process is a critical step in the ITPS design because the mass is very sensitive to the materials used, the lightest design being over 3 times lighter than the original reference design. The ranking of the different material combinations examined also showed that aluminosilicate/Nextel 720 composites (for TFS and web) and beryllium (for BFS) leads to the lightest ITPS design with a mass per unit area of 12.0 kg/m^2 (2.47 lb/ft^2). We found that, for identical thermal conditions, the ITPS based on this material combination is only about 40% heavier than a reference TPS-only design, sized at the same preliminary design phase as the ITPS and that considered the same corrugated core panel concept but without imposing any structural requirements (zero web thickness). However, whereas the TPS-only design provides only thermal protection, the ITPS concept was shown to be able to provide significant structural load bearing capabilities as well.

Appendix A: Variable Reduction for Thermal Analysis

To reduce computational cost and improve user-friendliness, we sought to reduce to a minimum the number of variables needed to express the maximum BFS temperature, if possible to only two variables. For this purpose, we used a combination of simplifying assumptions, dimensional analysis, and global sensitivity analysis, which led to a mildly simplified problem allowing us to condense the relevant material parameters into a small number of nondimensional parameters. To facilitate nondimensionalization, we made following simplifying assumptions:

1) The three thermal properties of the TFS (C_T, k_T, and ρ_T) have a negligible impact on the maximum BFS temperature, mainly due to the small thickness of the TFS (about 2.2 mm compared with a total ITPS thickness of about 120 mm). Consequently C_T, k_T, and ρ_T were removed from the relevant parameters influencing the BFS temperature.

2) The temperature is approximately constant through the BFS, because the BFS thickness is small (typically 5 mm thick compared with a total ITPS thickness of 120 mm) and its conductivity is about 1 order of magnitude higher than that of the homogenized core. This allows removing k_B from the relevant parameters and simplifying the boundary condition at the BFS.

3) The material properties were treated as constant (temperature independent). In the exact FE model (described in Sec. II.A), temperature dependence has been included for all materials, but the largest dependence was that of the Saffil® foam. Thus, in the simplified problem TFS, web, and BFS materials were assigned constant properties based on their nominal values given in the CES Selector 2005 material database [14]. The properties of the database materials used are also restated in Appendix B. For Saffil®, the material properties were assigned the values at a representative temperature chosen to minimize the difference between the maximum BFS temperature when using the constant values and the one when using temperature-dependent values for an ITPS design with the dimensions given in Table 2 and a Nextel (TFS), zirconia (web), aluminum (BFS) material combination. Because the representative temperature was determined for this fixed material combination, we tested the effects of varying the materials and found them to be small enough to use this representative temperature for the entire range of materials we consider.

Under these assumptions, the thermal problem is simplified as shown in Fig. A1 and its equations can be rewritten as follows.

Heat conduction equation:

$$k_C \frac{\partial^2 T(x,t)}{\partial x^2} = \rho_C C_C \frac{\partial T(x,t)}{\partial t} \quad \text{for } 0 < t < t_{\text{end}}$$

Initial condition:

$$T(x, t=0) = T_i$$

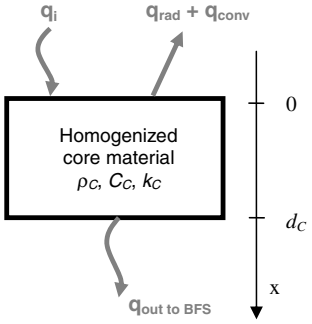

Fig. A1 Simplified thermal problem for dimensional analysis.

Boundary conditions:

$$q_{\text{out}} = -k_C \frac{\partial T(x,t)}{\partial x}\bigg|_{x=d_C} = \rho_B C_B d_B \frac{\partial T(x,t)}{\partial t}\bigg|_{x=d_C}$$

$$q_{\text{in}} = -k_C \frac{\partial T(x,t)}{\partial x}\bigg|_{x=0} = q_i(t) - \varepsilon\sigma T(0,t)^4 - h(t)T(0,t)$$

To nondimensionalize the equations of this problem, we used the Vaschy–Buckingham theorem (or Pi theorem) [16,17] and the following nondimensional variables were defined:

$$\frac{T}{T_i} = \Gamma \qquad \frac{x}{d_C} = \xi \qquad \frac{t}{t_{\text{end}}} = \tau \qquad \frac{k_C t_{\text{end}}}{d_C^2 \rho_C C_C} = \beta$$

$$\frac{d_B \rho_B C_B}{d_C \rho_C C_C} = \gamma \qquad \frac{d_C \varepsilon \sigma T_i^3}{k_C} = \kappa \qquad \frac{d_C q_i(t)}{k_C T_i} = \varphi(\tau)$$

$$\frac{h(t) d_C}{k_C} = Bi(\tau)$$

In terms of these nondimensional variables, the thermal problem can be written in the following nondimensional form:

Heat conduction equation:

$$\beta \frac{\partial^2 \Gamma}{\partial \xi^2} = \frac{\partial \Gamma}{\partial \tau} \quad \text{for } 0 < \tau < 1$$

Initial condition:

$$\Gamma(\xi, \tau = 0) = 1$$

Boundary conditions:

$$-\beta \frac{\partial \Gamma}{\partial \xi}\bigg|_{\xi=1} = \gamma \frac{\partial \Gamma}{\partial \tau}\bigg|_{\xi=1} \quad \text{and}$$

$$-\frac{\partial \Gamma}{\partial \xi}\bigg|_{\xi=0} = \varphi(\tau) - \kappa \cdot \Gamma(0,\tau)^4 - Bi(\tau) \cdot \Gamma(0,\tau)$$

The nondimensional temperature Γ can be expressed as a function of the nondimensional distance ξ, the nondimensional time τ, and five other nondimensional parameters. At the maximum BFS temperature, we are at a fixed location (because we ignore the BFS thickness) and are not interested in the time at which this maximum occurs. Accordingly, the maximum BFS temperature is independent of the nondimensional distance ξ and the nondimensional time τ.

The physical interpretation of the remaining five nondimensional parameters is the following. The Fourier number β is a nondimensional thermal diffusivity, that is, the ratio between the rate of heat conduction and the rate of heat storage (thermal energy storage) of the homogenized core; γ is the ratio between the heat capacity of the BFS and heat capacity of the homogenized core; κ is the ratio between the rate of radiation and the rate of heat conduction; and φ is the ratio between the incident heat flux and the rate of heat conduction, or it can be seen as a nondimensional heat flux. Finally Bi, the Biot number, is the ratio between the rate of convection and the rate of heat conduction.

The three nondimensional parameters κ, φ, and Bi are all proportional to d_C/k, whereas all the other parameters in κ, φ, and Bi are fixed in our study. Indeed, we are only interested in varying the materials and the geometry; the initial temperature T_i, the emissivity ε, the incident heat flux profile $q_i(t)$, and the convection film coefficient profile $h(t)$ are all fixed in the present study (see Fig. 3 for the profiles of $q_i(t)$ and $h(t)$ used). This means that for our purpose we can consider only one of these three nondimensional parameters, and we chose κ. Summing up, for the purpose of the material selection, the maximum BFS temperature can be expressed as a function of only three parameters: β, γ and κ.

From initial FE analyses, it seemed that the maximum BFS temperature was relatively insensitive to κ. To check this, we used 343 FE simulations (a $7 \times 7 \times 7$ grid in β, γ, and κ) and conducted a global sensitivity analysis using Sobol's approach [18]. We found that β accounts for 35.76% of the model variance and γ accounts for 64.18%, whereas κ accounts for only 0.06%. Thus, we can explain almost the entire behavior of the model with only the two variables β and γ.

From a physical point of view, the fact that κ has a negligible role can be explained as follows: κ is proportional to d_C/k, which is also present in β. That means that, if we want to change κ while keeping β constant, we need to also modify t_{end} (which is the only other variable in β that does not appear either in γ or in κ). If we increase κ by decreasing k_C, we need to also increase t_{end} by a certain amount to keep β constant. Decreasing k_C has the effect of lowering the BFS temperature, whereas increasing t_{end} has the effect of making it higher. From the global sensitivity analysis, it turns out that these two effects cancel each other out, which explains why κ has very little impact.

To find the limits of the simplifying assumptions that were considered to achieve this reduction in the number of variables, an antioptimization procedure was carried out, the details of which are provided in [19]. The antioptimization process looks to find the places with the highest error in using an approximation in terms of the reduced number of variables. By looking at the designs corresponding to the antioptimum, we can understand what causes these errors. This procedure showed that the approximation in terms of the reduced number of variables has poor accuracy when the geometry is far away from the one for which the representative temperature of the core was established (see assumption 3 at the beginning of this Appendix). For these unusual geometries, the representative temperature shifts due to temperature dependence of the core. This temperature shift is poorly accounted for by the approximation, which explains the poor accuracy for these geometries. To further improve the accuracy of the temperature approximation for a large range of geometries, we would have to add nondimensional parameters that account for the temperature dependence. For the geometries for which we used the approximation in terms of the reduced number of variables in this paper, it was found that the errors are acceptable (a maximum error of less than about 10 K). Additional details on testing and validation are also provided in Sec. II.B.

Appendix B: Properties of Candidate Materials

The material properties of the candidate materials for the web, BFS, and TFS are provided in Tables [B1–B3], respectively. The material properties come from the CES Selector 2005 material database [14]. The ranges of the material properties are due to uncertainty in identifying them or to variations due to different possible manufacturing processes.

Table B1 Selected web materials properties

Designation		Titanium alpha-beta alloy Ti–6Al–4V (STA)	Zirconia (HTZ)	Aluminosilicate/Nextel 720 fiber composite, quasi-isotropic woven
Mechanical properties				
Density	kg/m^3	4407–4451	6080–6210	2450–2600
Young's modulus	GPa	110–117	209.7–220.4	133.5–139.1
Compressive strength	MPa	758–1117	1429–1575	67.9–68.8
Tensile strength	MPa	896–1138	142.9–157.5	67.9–68.8
Fracture toughness	$MPa \cdot m^{0.5}$	82–100	15–20	40.5–47.6
Poisson's ratio		0.31–0.32	0.24–0.31	0.23–0.25
Shear modulus	GPa	43–45.21	82.25–86.4	54.15–55.64
Thermal properties				
Max. service temp.	K	630–672	1248–1298	1273–1373
Melting point	K	1878–1933	2823–2973	1273–1373
Specific heat	$J/kg \cdot K$	553–575.6	418–436	950–1100
Thermal conductivity	$W/m \cdot K$	7.3–7.9	1.8–1.9	2.52–2.93
Thermal expansion	$\mu strain/K$	9–9.46	7.8–8.1	5.745–5.745
Price (2005 USD)	USD/kg	28.28–47.13	16.97–24.51	4807–5750

Table B2 Selected BFS materials properties

Designation		Cast aluminum alloy	Epoxy/carbon fiber quasi-isotrop. laminate	Beryllium, grade S-200F, vacuum hot pressed
Mechanical properties				
Density	kg/m^3	2570–2950	1550–1580	1840–1860
Young's modulus	GPa	68–88.5	49.7–60.1	290–315
Compressive strength	MPa	30–280	542.1–656.8	250–365
Tensile strength	MPa	75–360	248.6–355.9	320–430
Fracture toughness	$MPa \cdot m^{0.5}$	18–35	6.12–87.61	10–14
Poisson's ratio		0.32–0.36	0.305–0.307	0.06–0.075
Shear modulus	GPa	25–34	19–23.01	134–150
Thermal properties				
Max. service temp.	K	403–473	413–493	803–1103
Melting point	K	723–980	373–453	1545–1565
Specific heat	$J/kg \cdot K$	944–982	901.7–1037	1820–1930
Thermal conductivity	$W/m \cdot K$	80–220	1.28–2.6	190–216
Thermal expansion	$\mu strain/K$	16–24	0.36–4.02	10–12
Price (2005 USD)	USD/kg	1.42–2.3	58.48–72.05	735.2–867.1

Table B3 Selected TFS materials properties (note that carbon–carbon composites were not selected for the geometry optimization study of Sec. IV due to their low fracture toughness; their properties are nevertheless listed for information purposes)

Designation		Nickel–chromium alloy, Inconel 718	Aluminosilicate/Nextel 720 fiber composite, quasi-isotropic woven	Carbon fiber carbon matrix composite
Mechanical properties				
Density	kg/m^3	8150–8300	2450–2600	1440–1720
Young's modulus	GPa	195–205	133.5–139.1	8.3–100
Compressive strength	MPa	1010–1240	67.9–68.8	17–247
Tensile strength	MPa	1220–1510	67.9–68.8	6.9–34.5
Fracture toughness	$MPa \cdot m^{0.5}$	120–150	40.5–47.6	5.7–6.3
Poisson's ratio		0.28–0.3	0.23–0.25	0.31–0.35
Shear modulus	GPa	73–81	54.15–55.64	3.2–34
Thermal properties				
Max. service temp.	K	1130–1255	1273–1373	2275–2325
Melting point	K	1533–1610	1273–1373	3473–3673
Specific heat	$J/kg \cdot K$	410–455	950–1100	754–1700
Thermal conductivity	$W/m \cdot K$	10.5–12.5	2.52–2.93	10–87
Thermal expansion	$\mu strain/K$	11.5–13.5	5.745–5.745	0.2–8.4
Price (2005 USD)	USD/kg	13.2–26.39	4807–5750	188.5–207.4

Acknowledgments

The authors would like to thank Max Blosser from NASA Langley Research Center for his valuable input during the teleconferences we had. They also thank Tushar Goel for his assistance with the global sensitivity analysis. Finally, they gratefully acknowledge financial support from the NASA Constellation University Institutes Project (formerly University Research Engineering and Technology Institutes) grant NCC3-994 to the Institute for Future Space Transport at the University of Florida. The cognizant program managers are Claudia Meyer and Jeffry Rybak at the NASA John H. Glenn Research Center at Lewis Field.

References

[1] Erb, R. B., Greenshields, D. H., Chauvin, L. T., Pavlosky, J. E., and Statham, C. L., "Apollo Thermal-Protection System Development," *Journal of Spacecraft and Rockets*, Vol. 7, No. 6, June 1970, pp. 727–734.
doi:10.2514/3.30027

[2] Olynick, D., Chen, Y. K., and Tauber, M. E., "Forebody TPS Sizing with Radiation and Ablation for the Stardust Sample Return Capsule," AIAA Paper 1997-2474, June 1997.

[3] Cooper, P. A., and Holloway, P. F., "The Shuttle Tile Story," *Astronautics and Aeronautics*, Vol. 19, No. 1, Jan. 1981, pp. 24–34.

[4] Freeman, D. C., Talay, T. A., and Austin, R. E., "Reusable Launch Vehicle Technology Program," *Acta Astronautica*, Vol. 41, No. 11, 1997, pp. 777–790.
doi:10.1016/S0094-5765(97)00197-5

[5] Baumgartner, R. I., "Venturestar^{TM} Single Stage to Orbit Reusable Launch Vehicle Program Overview," *AIP Conference Proceedings Space Technology and Applications International Forum*, Vol. 387, American Institute of Physics, College Park, MD, Jan. 1997, pp. 1033–1040.

[6] Blosser, M. L., Chen, R. R., Schmidt, I. H., Dorsey, J. T., Poteet, C. C., Bird, R. K., and Wurster, K. E., "Development of Advanced Metallic, Thermal-Protection-System Prototype Hardware," *Journal of Spacecraft and Rockets*, Vol. 41, No. 2, March–April 2004, pp. 183–194.
doi:10.2514/1.9179

[7] Poteet, C. C., Abu-Khajeel, H., and Hsu, S.-Y., "Preliminary Thermal-Mechanical Sizing of a Metallic Thermal Protection System," *Journal of Spacecraft and Rockets*, Vol. 41, No. 2, Mar–Apr 2004, pp. 173–182.
doi:10.2514/1.9174

[8] Kim, W. Y., Grandhi, R. V., and Haney, M., "Multi-Objective Evolutionary Structural Optimization Using Combined Static/Dynamic Control Parameters," *AIAA Journal*, Vol. 44, No. 4, April 2006, pp. 794–802.
doi:10.2514/1.16971

[9] Bapanapalli, S. K., Martinez, O. M., Gogu, C., Sankar, B. V., Haftka, R. T., and Blosser, M. L., "Analysis and Design of Corrugated Core Sandwich Panels for Thermal Protection Systems of Space Vehicles," AIAA Paper 2006-1942, 2006.

[10] Martinez, O., Bapanapalli, S. K., Sankar, B. V., Haftka, R. T., and Blosser, M. L., "Micromechanical Analysis of Composite Truss-Core Sandwich Panels for Integral Thermal Protection Systems," AIAA Paper 2006-1876, 2006.

[11] ABAQUS/Standard User's Manual, Ver. 6.5.1, Hibbitt, Karlsson, and Sorensen, Inc., Pawtucket, RI, 2004.

[12] Williams, S. D., and Curry, D. M., "Thermal Protection Materials," NASA RP-1289, 1992.

[13] Myers, D. E., Martin, C. J., and Blosser, M. L., "Parametric Weight Comparison of Advanced Metallic, Ceramic Tile, and Ceramic Blanket Thermal Protection Systems (TPS)," NASA TM-2000-210289, 2000.

[14] CES Selector Edupack 2005, Granta Design Limited, Cambridge, England, UK, 2005.

[15] Anon., "Columbia Accident Investigation Board Report," NASA, Washington, DC, 2003.

[16] Vaschy, A., "Sur les Lois de Similitude en Physique," *Annales Télégraphiques*, Vol. 19, 1892, pp. 25–28.

[17] Buckingham, E., "On Physically Similar Systems; Illustration of the Use of Dimensional Equations," *Physical Review*, Vol. 4, 1914, pp. 345–376.
doi:10.1103/PhysRev.4.345

[18] Sobol, I. M., "Sensitivity Estimates for Nonlinear Mathematical Models," *Mathematical Modeling and Computational Experiment*, Vol. 1, Wiley, New York, 1993, pp. 407–414.

[19] Gogu, C., Bapanapalli, S. K., Haftka, R. T., and Sankar, B. V., "Comparison of Materials for Integrated Thermal Protection Systems for Spacecraft Reentry," AIAA Paper 2007-1860, April 2007.

K. Wurster
Associate Editor